Exploring solar cell performance of inorganic absorber layer of Cs_2TiBr_6 and $CH_3NH_3SnBr_3$ perovskite: A numerical study

[1]Anchal Srivastava,[1]Navina Wadhwani,[1]Nidhi Singh, [2]K. C. Dubey, and[1]R. K. Shukla

[1]Department of Physics, University of Lucknow, Lucknow-226007
[2]Department of Physics, Shia PG College, Lucknow-226020

Email: rajeshkumatshukla00@gmail.com

Abstract
In the perovskite based solar cells, hazardous lead (Pb) is engaged as an absorber layer, while an unstable polymer is used as the electron/hole transport layer. Despite its enticing features, the device's use of lead and biodegradable components has to be addressed. The halide-based perovskite offers various advantages, including high efficiency, ease of production, and low cost. Lead-free titanium-based inorganic perovskite solar cells (PSCs) have sparked widespread scientific consideration in current years as a means of mitigating the potentially negative environmental impacts of lead exposure. Titanium is non-toxic, strong, affordable, and abundantly available when compared to other elements. The SCAPS-1D software simulates and optimizes the performance of PSCs. This work investigated the effect of various TiO_2 and NiO parameters as charge transport materials on the absorber double layer of Cs_2TiBr_6 and $CH_3NH_3SnBr_3$PSCs. After numerically optimizing the perovskite layer thickness, defect density, doping concentration and other device input parameters, a greatly efficient PSC with PCE of 28.92%, V_{OC} of 1.2999 V, J_{SC} of 24.63 mA.cm^{-2}and fill factor of 90.32% is obtained. The findings are highly encouraging, demonstrating the promise of Cs_2TiBr_6/$CH_3NH_3SnBr_3$ for efficient and environmentally friendly solar applications. The findings of this work are anticipated to not only improve understanding, but also encourage additional research into lead-free PSCs.
Keywords: Solar cell, Perovskite, HTL, ETL, Cs_2TiBr_6 and $CH_3NH_3SnBr_3$.

Introduction: Access to inexpensive energy sources is crucial for sustainable social and economic development [1]. In today's world, energy demand is steadily increasing. According to Das et al.[2], the world is becoming more industrialized and has higher living standards. The majority of energy comes from scarce and polluting fossil resources. Numerous energy sources have been created to address rising energy demand. Solar energy is the most practical approach in this situation [3-4]. Improving solar cell efficiency can help meet global energy demand, especially in underdeveloped countries. Photovoltaic cells areused to generate direct current using the solar irradiation incident upon it [5].PSCs have proven to be amongst the most promising. Power conversion efficiency (PCE) of more than 25% on single junction architecture is challenging to achieve when using a typical silicon solar cell that is nearing commercialization. Only over fifteen years after its inception. However, there are a few severe concerns that must be addressed before PSC can be

industrialized, such as device stability in the air underneath lighting and the toxicity of the chemicals utilized. Almost so far successful compositions for perovskite solar cells Methylammonium (CH_3NH_3 +) (MA), formamidinium (NH_2CHNH_2 +) (FA), and A cation site cesium (Cs +), B cation site lead (Pb), and ABX_3 Perovskite structure X anion site iodine (I), bromine (Br).However, the presence of harmful heavy metals like lead is linked to it. The entire life cycle of perovskite solar cells raises significant environmental concerns. As a result, the next high efficiency, more research communities and industrialists question its future, opening the road for lead-free perovskite material. That is why researchers are attempting to investigate lead-free perovskite materials for solar cells. Many lead-free perovskite absorbers have a large bandgap and are appropriate for replacement. Further improvements in tin-based perovskite solar cells can be made by optimizing a diversity of parameters and device designs, which can serve as a foundation for future research. This simulation effort controlled to the progress of a perovskite based on Cs_2TiBr_6 and methylammonium tin bromide ($CH_3NH_3SnBr_3$)[6-12]. The thickness and doping levels of several layers, including as the electron transport layer, absorber layer, and hole transport layer, have been changed, and the repercussions have been inspected for further performance development. Defect densities have also been enhanced. The maximum possible efficiency is 28.92%, the highest documented to date.

Methodology:

Simulation software:Simulation of solar cell device performance is critical for optimizing a novel material device. Because building a solar cell is both complicated and time-consuming, simulations of the proposed structure can forecast performance and dependability prior to construction. SETFOS, SILVACO, ATLAS, AMPS, COMSOL, and SCAPS-1D are the software tools that can be used to simulate cell properties based on device input parameters [13]. Researchers from Gent University's (Ghent, Belgium) Department of Electronics and Information Systems developed SCAPS-1D as a numerical simulation application. The SCAPS solves three equations to determine device properties: Poisson's, electron/hole transport, and hole continuity [14].

Mathematical modelling: The SCAPS-1D simulator simulates semiconductor devices by solving the Poisson's equation, the electron continuity equation, and the hole continuity equation. SCAPS-1D software solves three partial differential equations to determine electron and hole concentrations in electrostatic potentials based on $\times$ [15].This simulation project involved much study. Cs_2TiBr_6/$CH_3NH_3SnBr_3$ is a light-absorbing substance. Unlike lead-based perovskites, it is non-toxic. $CH_3NH_3SnBr_3$ may be a feasible, high-contrast alternative to $CH_3NH_3PbX_3$. The simulation's configuration is the most crucial components. This task will run a device simulation. The cleavage configuration of FTO/TiO_2/Cs_2TiBr_6/$CH_3NH_3SnBr_3$/NiO/Au is depicted in Figure 1. Light passes through the FTO edge, and Cs_2TiBr_6/$CH_3NH_3SnBr_3$ is used as the main light absorption layer sandwiched Fluoride-doped tin oxide (FTO) serves as the front and rear metal contacts between ETL and HTL gold (Au). TiO_2 is suitable ETL candidate for solar cell [16-21].This research focuses on simulating configurations and varied attributes. The thickness of the different layers is inputted during thesimulation. Doping concentration, effective state density of the conduction band (CB), and valence band (VB) all fluctuate. Investigate the optimal optical and electrical attributes for realizing high PCE.

Solar cell structure:The spectrum of solar limits the yield of a single solar cell, but this can be enhanced by stacking two separate band gaps that can absorb higher energy photons at the top and lower energy photons at the bottom. Figure 1 displays the proposed solar cell structure, FTO/TiO_2/Cs_2TiBr_6/$CH_3NH_3SnBr_3$/Au. The suggested solar cell is lighted by the conventional AM 1.5 G1 sun through an FTO transparent layer.

Au (Backside Anode)
NiO (Hole Transport Layer)
CH₃NH₃SnBr₃ (Absorber Layer)
Cs₂TiBr₆ (Absorber Layer)
TiO₂ (Electron Transport Layer)
FTO (Front Contact)

Light Incident

Fig. 1: Schematic structure of FTO/TiO₂/Cs₂TiBr₆/CH₃NH₃SnBr₃/Au-based solar cell. Photovoltaic devices have three main parts: Light absorber Charge carriers are layers that transform incident photons into electrons and holes; carrier collectors capture carriers; and metal contacts transport charge carriers to an external circuit. The absorber utilized here is Cs₂TiBr₆/CH₃NH₃SnBr₃. The simulation was based on numerous prior research articles. These references are cited. Table 1 lists the following values: Considered when developing the fundamental configuration simulation method to achieve optimal results through variations.

Table 1: Values representing the material properties used in the simulation.

Physical Parameters	Symbol	Unit	NiO (HTL)	CH₃NH₃SnBr₃	Cs₂TiBr₆	TiO₂ (ETL)
Thickness	Th	nm	150	400	400	50
Energy Band Gap	E_g	eV	3.6	1.3	1.8	3.26
Electron Affinity	X	eV	1.8	4.17	4.47	4.2
Dielectric Permittivity (Relative)	ε_r	-	11.7	10	10	10
Density of States at Valence Band	N_V	cm⁻³	2.5×10^{20}	1.8×10^{18}	6×10^{19}	1.8×10^{18}
Density of States at Conduction Band	N_C	cm⁻³	2.5×10^{20}	2.2×10^{18}	2×10^{19}	2.2×10^{18}
Hole Thermal Velocity	V_e	cm/s	1×10^7	1×10^7	1×10^7	1×10^7
electron Thermal Velocity	V_h	cm/s	1×10^7	1×10^7	1×10^7	1×10^7
Electron Mobility	μ_e	cm²/V.s	2.8	1.6	4.4	20
Hole Mobility	μ_h	cm²/V.s	2.8	1.6	2.5	10
Uniform Shallow	ND	cm⁻³	0	1×10^{13}	1×10^{19}	1×10^{17}

Donor Doping						
Uniform Shallow Acceptor Doping	NA	cm^{-3}	3×10^{18}	1×10^{13}	1×10^{19}	0
Defect Density	N_t	cm^{-3}	1×10^{15}	1.5×10^{15}	1.5×10^{15}	1×10^{15}
References			22	23	24	25

Result and Discussion: Before improving each aspect that influences the power conversion efficiency of PSCs, the baseline parameters for the PSC device were determined. These included a 50 nm ETL layer of TiO$_2$, a 400 nm Absorber layer (of Cs$_2$TiBr$_6$ and CH$_3$NH$_3$SnBr$_3$), and a 150 nm HTL layer of NiO. At AM 1.5G, the device worked with a continuous illumination of 1000 W/m^2 at 300 K. Table 2 shows the initial values for V$_{oc}$,J$_{sc}$,FF andPCE.

Table 2: Solar cell initial parameters for the FTO/TiO$_2$/Cs$_2$TiBr$_6$/CH$_3$NH$_3$SnBr$_3$/Au PSC structure.

V$_{oc}$	J$_{sc}$	FF	PCE
0.9187 V	31.32 mA/cm^2	62.02%	17.84%

Effect of ETL (TiO$_2$) layer thickness: The major function of the ETL layer is to transport electrons from the absorber layer to the FTO while inhibiting them from recombining with holes within the absorber layer [26]. The thickness of ETL is critical to achieving optimal performance. Because ETL thickness increases, so the series resistance, and therefore recombination occur. The thickness of the ETL layer is adjusted from 10 to 500 nm. Figure 2 shows that V$_{oc}$, J$_{sc}$, FF and PCE stay nearly constant. The thickness of the TiO$_2$ layer has no discernible impact on the PSC output, which is consistent with previous study [27]. This is because TiO$_2$ has a comparatively high electron mobility, which allows electrons to be easily transported through even thin ETL layers. The low band gap also decreases the ETL layer's resistance. Therefore, the ETL thickness of 10nm is chosen as optimal.
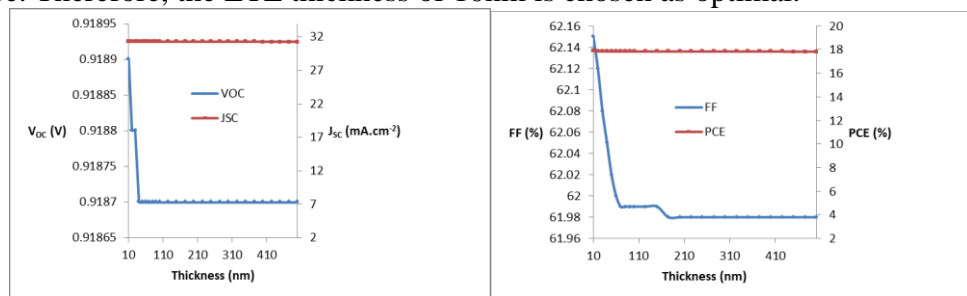

Fig. 2: Effect of ETL layer thickness on (a) V$_{oc}$&J$_{sc}$, (b) PCE & FF.

Effect of shallow donor density of ETL (TiO$_2$): To achieve optimal performance, donor density is set between 10^9 and 10^{22} cm^{-3}. Numerousinvestigation groups have workingof doping to raise the charge mobility and electron diffusion length of TiO$_2$. Figure 3 indicates that when the donor density of TiO$_2$ sheets is suitably enough (10^{20}cm^{-3}), PCE increases by 17.90%. The rising trend in PCE is due to increased FF at the same donor density (10^{20} cm^{-3}). Furthermore, changing donor density has no discernible effect on V$_{oc}$ or J$_{sc}$. This increase in PCE is attributed to more effective charge carrier collection and transfer, rather than more charge carriers manufactured or collected [28].
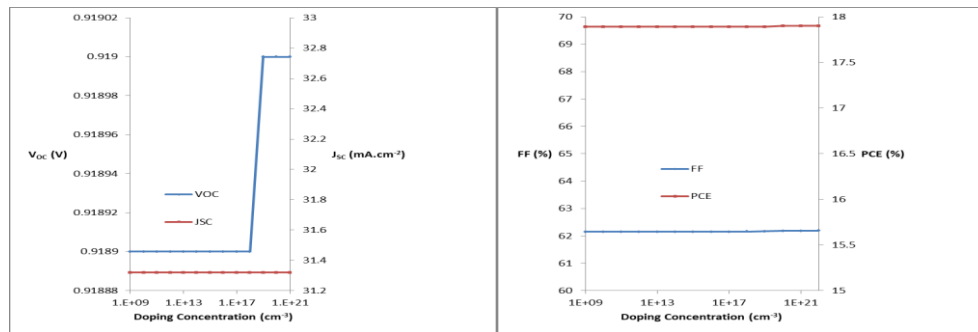
Fig. 3: Effect of shallow donor density of ETL layer on (a) V_{oc} & J_{sc}, (b) PCE & FF.

Effect of defect density (N_t) of ETL (TiO2): The trap density of states (N_t) in the TiO2 layer was modified from 10^9 to 10^{22} cm^{-3} to evaluate its impact on the efficiency of the proposed PSC architecture. Figure 4 shows how this N_t modification in the ETL (TiO2) affects the photovoltaic parameters. The graph shows that V_{oc}, J_{sc}, FF and PCE remain constant when N_t increases to 10^{22} cm^{-3}.
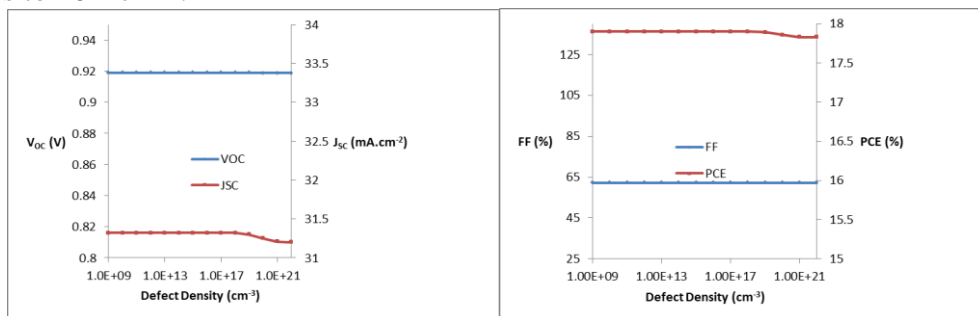

Fig.4: Effect of defect density N_t in TiO2 layer on (a) V_{oc} & J_{sc}, (b) PCE & FF.

Effect of thickness of absorber layer Cs2TiBr6: The thickness of the absorber layer significantly affects the solar cell's performance, including V_{oc}, J_{sc}, FF, and PCE. The solar cell absorber layer absorbs photon energy and transports photo-induced electron and hole carriers to the cell's collecting electrodes [29]. The physical properties of the absorber layer have a considerable impact on the efficient generation and extraction of photo-generated carriers. After a particular layer thickness, the absorber layer may become saturated with high wavelength photon absorption, resulting in near-constant PV performance. The film structure has a noteworthy impact on the durability and diffusion length of photo-generated carriers, which in turn affect the absorber layer's quality. The PCE of a solar cell is calculated using two factors: carrier movement and light absorption. Light absorption becomes a big concern when the absorption layer is very thin. This is owing to the ease with which the produced carrier can contact the electrode. However, as the thickness exceeds a certain threshold, optical absorption approaches saturation. As a consequence, carrier transportation becomes essential. The thickness of this layer should be carefully calculated in order to absorb the maximum protons while limiting reverse saturation current. To determine the appropriate thickness of Cs2TiBr6 was varied from 250 nm to 1500 nm. Fig. 5 illustrates the effects of absorber layer thickness on PSC performance. The results in Fig. 5 show that increasing the absorber layer thickness reduces the current density, V_{oc}, PCE, and FF. The J_{sc} decreases from 31.20 mA/cm^2 to 30.15 mA/cm^2 as the layer thickness increases from 250 to 1500 nm. However, the PCE decreases from 18.54% to 10.92%, V_{oc} from 0.9276 V to 0.8945 V, and FF from 64.06% to 40.70%. This change is due to increased absorber thickness, which increases recombination and saturation current [30].
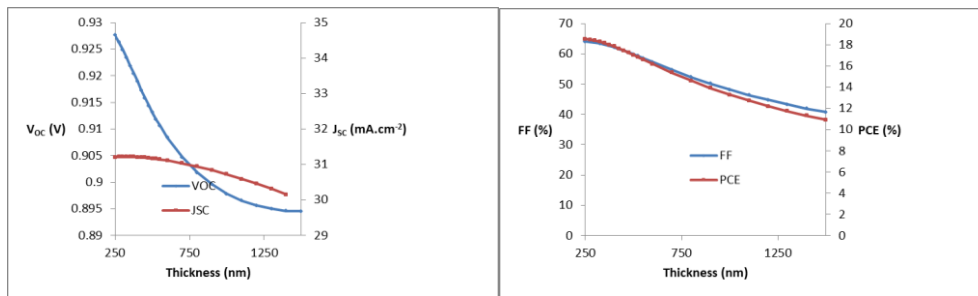
Fig. 5.Effect of absorber layer thickness of Cs_2TiBr_6 on (a) V_{oc}&J_{sc}, (b) PCE & FF.

Effect of Doping Concentration (N_D) of Absorber Layer Cs_2TiBr_6: In this investigation, we investigate the effects of varying the concentration of Uniform Shallow Donors within the initial absorber layer. Our experiment includes calculating various photovoltaic characteristics while modifying the Uniform Shallow Donor concentration between 10^9 and 10^{19} cm^{-3}, with the goal of defining the ideal value for the Cs_2TiBr_6 layer. The results, which include open-circuit voltage, short-circuit current, FF, and PCE, are shown in Fig. 6. The figure shows how changing the Uniform Shallow Donor concentration affects photovoltaic parameters like open-circuit voltage, short-circuit current, and fill factor. A maximum PCE (~18.54%) is achieved at a Uniform Shallow Donor concentration of 1×10^{19} cm^{-3} within the first absorber layer Cs_2TiBr_6.
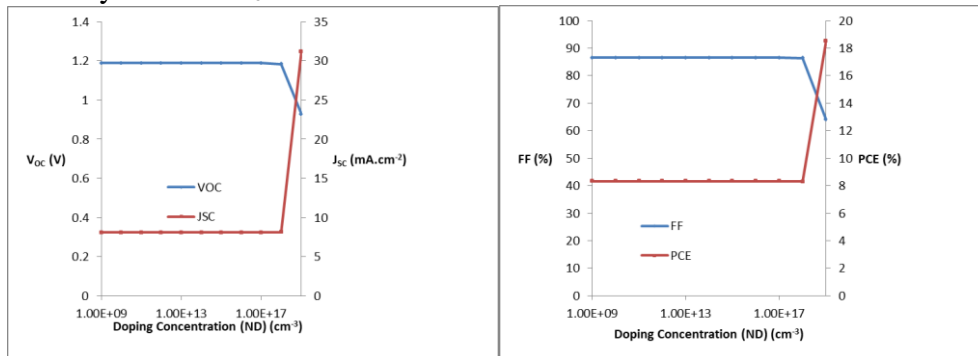

Fig. 6: V_{oc},J_{sc},FF andPCE of first absorber layer Cs_2TiBr_6 as a function ofUniform Shallow Donor Doping in proposed solar cell.

Effect of Doping Concentration (N_A) in (Cs_2TiBr_6) Absorber Layer: In this part, we investigate the effect of varying the concentration of Uniform Shallow Acceptors within the first absorber layer. Our analysis entails computing photovoltaic parameters while altering the Uniform Shallow Acceptor concentration from 10^{19} to 10^{22} cm^{-3}, with the goal of determining the best value for the Cs_2TiBr_6 absorber layer in the proposed solar cell. The results, which include V_{oc}, J_{sc}, FF and PCE, are shown in Fig.7. The figure shows that changing the Uniform Shallow Acceptor concentration affects photovoltaic parameters like open-circuit voltage, short-circuit current, and fill factor. The maximum PCE (~18.54%) was achieved at a concentration of 10^{19} cm^{-3} within the absorber layer.
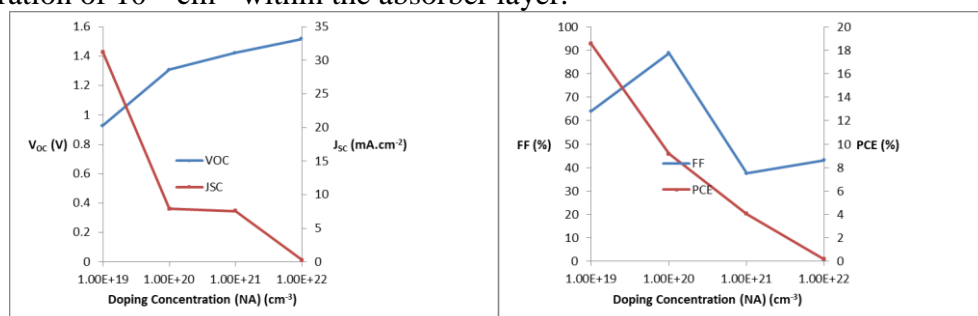

Fig.7: V_{oc}, J_{sc}, FF and PCEof first absorber layer as a function ofUniform Shallow Acceptor Doping inCs_2TiBr_6.

Effect of Defect Density (N_t)inCs$_2$TiBr$_6$ (Absorber Layer): The initial N_t value within this layer is set to 10^{15} cm^{-3}. Fig. 8 represents the link between PV parameters and N_t within the absorber layer. Significant improvements in the PV characteristics of the PSC are found when the N_t concentration in the perovskite lowers, which is reliable with conclusions from earlier investigations on lead perovskites. At a defect density of 1×10^9 cm^{-3}, the cell's PV characteristics significantly increase, with a J_{sc} of 31.27 mA/cm^2, V_{oc} of 1.9351V, FF of 64.93%, and PCE of 18.99%. The defect density is tuned at 1×10^9 cm^{-3}, allowing all PV parameters (V_{oc}, J_{sc}, FF and PCE) to approach maximum levels.
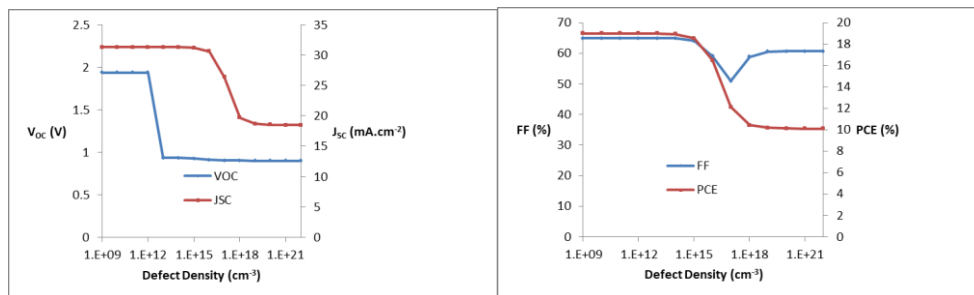

Fig.8: Illustrates the variation of PV parameters with defect density (N_t) of first absorber layerCs$_2$TiBr$_6$.

Optimization of second Absorber Layer Thickness (CH$_3$NH$_3$SnBr$_3$): Similarly, the layer thickness of CH$_3$NH$_3$SnBr$_3$ is varied from 400 nm to 1500 nm to determine the optimum thickness. Figure 9 illustrates the effects of absorber layer thickness on PSC performance. The results in Fig. 9 show that increasing the absorber layer thickness increases only current density while decreasing V_{oc}, PCE, and FF. The J_{sc} increases from 31.27 mA/cm^2 to 34.37 mA/cm^2 as the layer thickness grows from 400 to 1500 nm. However, the PCE decreases from 18.99% to 14.98%, V_{oc} from 0.9351 V to 0.9019 V, and FF from 64.93% to 48.33%.
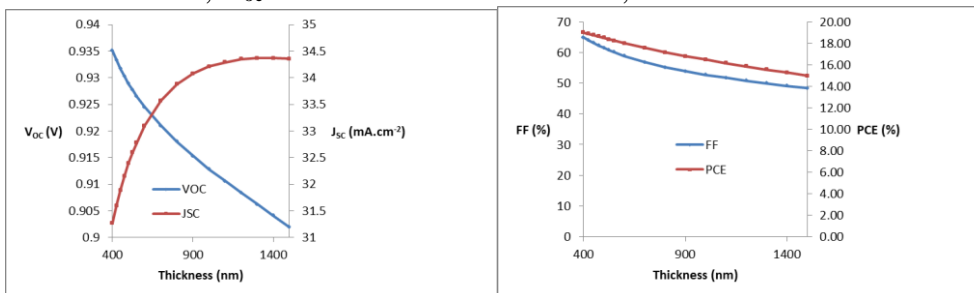

Fig. 9: Effect of absorber layer thickness on (a) V_{oc}&J_{sc}, (b) PCE & FF.

Effect of doping concentration (N_D) CH$_3$NH$_3$SnBr$_3$ of second Absorber Layer: Figure 10 displays that setting the doping concentration of the second Absorber Layer (CH$_3$NH$_3$SnBr$_3$) to 1×10^{22} yields a maximum PCE of around 28.92% for the cell. The software is then updated to reflect the revised doping concentration value for the second Absorber Layer (CH$_3$NH$_3$SnBr$_3$). The doping concentration of the second Absorber Layer (CH$_3$NH$_3$SnBr$_3$) is approximated between 1×10^{19} to 1×10^{22} cm^{-3} utilizing photovoltaic metrics such as V_{OC}, J_{SC}, FF, and PCE, as given in Fig. 10.
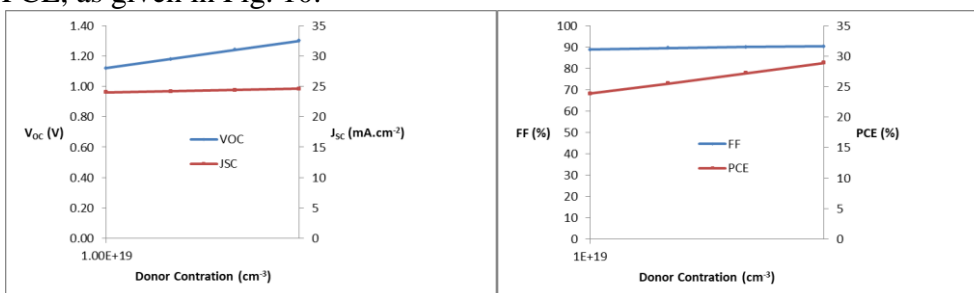
Fig.10: V$_{oc}$, J$_{sc}$, FF and PCEof second absorber layer CH₃NH₃SnBr₃ as a function ofUniform Shallow Donor Doping in proposed solar cell.

Effect of doping concentration (N$_A$) in (CH₃NH₃SnBr₃) second Absorber Layer: In this part, we investigate the effects of varying the concentration of Uniform Shallow Acceptors within the second absorber layer. Our research comprises analysing photovoltaic properties while adjusting the Uniform Shallow Acceptor concentration between 10^9 and 10^{22} cm^{-3}, with the goal of determining the best value for the CH₃NH₃SnBr₃ absorber layer in the proposed solar cell. The results, including V$_{OC}$, J$_{SC}$, FF, and PCE, are shown in Figure 11. The figure shows how changing the Uniform Shallow Acceptor concentration affects photovoltaic parameters like open-circuit voltage, short-circuit current, and fill factor. The maximum PCE (~28.92%) was achieved at a concentration of 10^9 cm^{-3} within the second absorber layer.
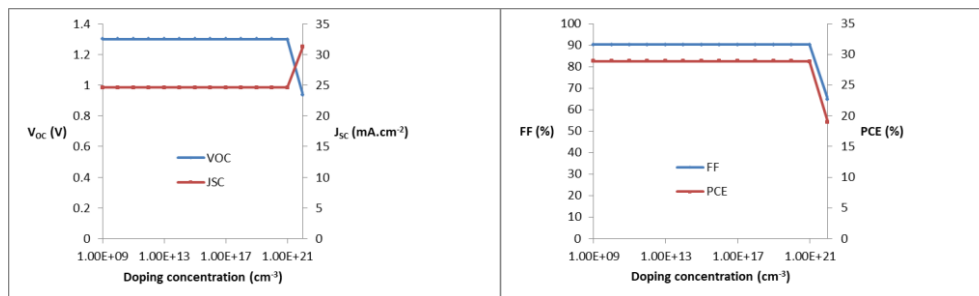
Fig.11: V$_{oc}$, J$_{sc}$, FF and PCEof second absorber layer as a function ofUniform Shallow Acceptor Doping inCH₃NH₃SnBr₃.

**Effect of Defect Density (N$_t$)inCH₃NH₃SnBr₃ (Absorber Layer):** The initial Nt value in the second absorber layer is set to 10^{15} cm^{-3}. Fig. 12 illustrates the relationship between PV parameters and N$_t$ in the second absorber layer. Significant improvements in the PV characteristics of the PSC are originate when the N$_t$ content of the perovskite drops, which is steady with findings from earlier experiments on lead perovskites. At a defect density of 1.0×10^{15} cm^{-3}, the cell's PV properties significantly improve, obtaining a J$_{sc}$ of 24.63 mA/cm^2, V$_{oc}$ of 1.2999 V, FF of 90.32%, and PCE of 28.92%. The defect density is optimized to 1.0×10^{15} cm^{-3}, allowing all PV parameters (V$_{oc}$, J$_{sc}$, FF and PCE) to approach maximum levels.
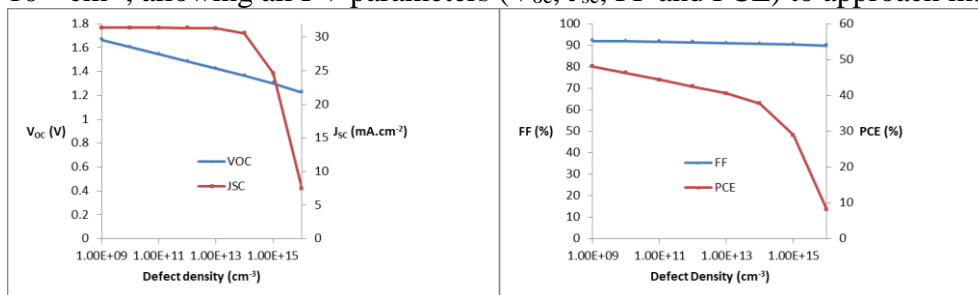
Fig.12: Illustrates the variation of PV parameters with defect density (N$_t$) of second absorber layerCH₃NH₃SnBr₃.

Influence of HTL (NiO) layer thickness: The primary function of an HTL layer is to accumulate holes while reducing recombination at the back contact. It also promotes holemovement from the absorber layer to the rear contact [31]. A larger HTL layer gives holes a longer path to back contact, reducing the possibility of recombination. While optimizing the HTL layer thickness, the absorber and ETL layer thicknesses are kept constant. In this study, the thickness of an HTL layer is adjusted from 10 to 500 nm. Figure 13 illustrates that changing the HTL thickness has no role on the V$_{oc}$ or the fill factor. A thicker HTL layer has a larger series resistance, which might reduce the solar cell's efficiency. However, to limit the chance of recombination, HTL must have a thicker layer than ETL.
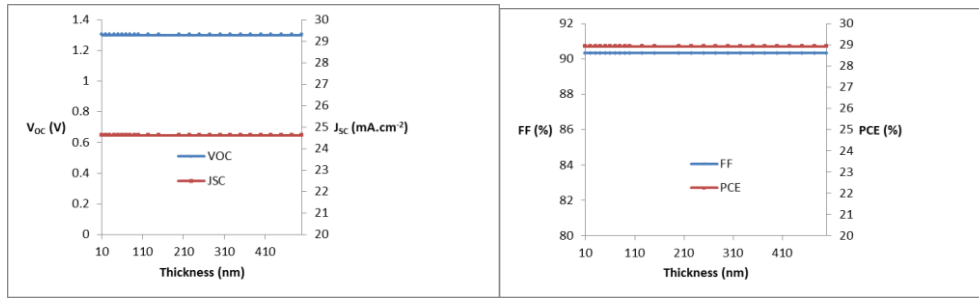
Fig. 13:Influence of HTL layer thickness on V$_{oc}$, J$_{sc}$, FF and PCE.

Influence of Acceptor Density of HTL (NiO): Acceptor density was increased from 1×109 to 1×10^{21} cm^{-3} to enhance performance. A comparable rise in PCE is observed. Figure 14 indicates that the values of all parameters remained constant as the value of acceptor density rose. However, the greatest value of PCE was found to be 28.92% when the optimum value of N$_A$ was chosen to be 1×10^{17}. Higher values of NA can create coulomb traps, resulting in lower hole mobility [32]. The suggested cell has V$_{oc}$, J$_{sc}$, FF and PCEvalues of1.2999 V, 24.63 mA/cm^2,90.32% and28.92%, when NA of HTL is 1×10^{17}cm^{-3}.
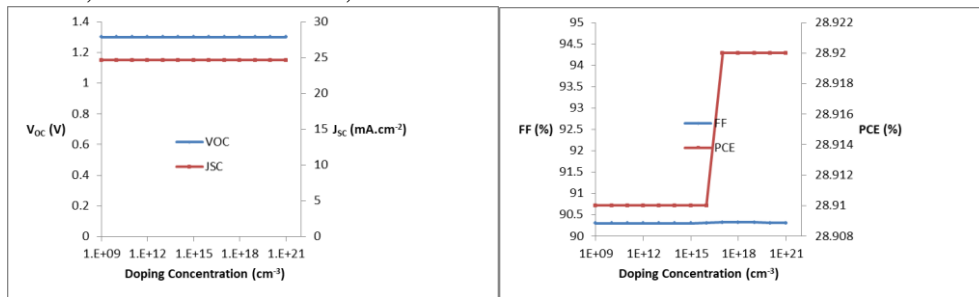
**Fig. 14:Influence of acceptor density of HTL layer on V$_{oc}$, J$_{sc}$, FF and PCE.**

Influence of Defect Density of HTL (NiO): The trap density of states (N$_t$) in the NiO layer was modified from 10^9 to 10^{22} cm^{-3} to evaluate the overall power efficiency of the proposed PSC architecture. The effect of this N$_t$alteration in the HTL (NiO) on the photovoltaic parameters is seen in figure 15. The graph shows that V$_{oc}$, J$_{sc}$, FF and PCE remain constant when N$_t$ increases to 10^{22} cm^{-3}.
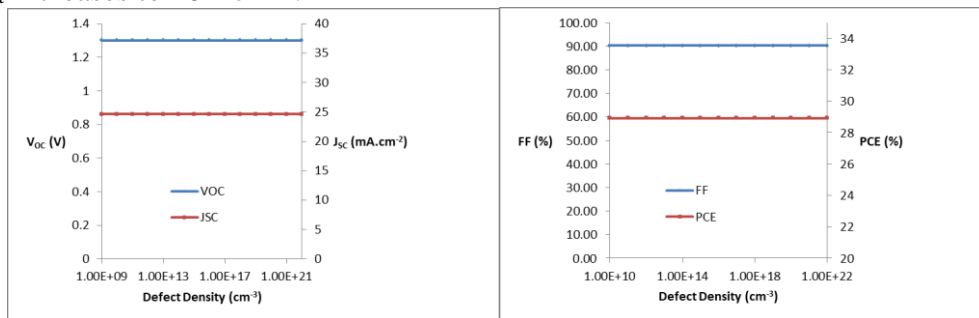
Fig.15: Influence of defect density N$_t$ in NiO layer on theV$_{oc}$, J$_{sc}$, FF and PCE of the proposed solar cell.

Effect of temperature: The solar cell's production is strongly reliant on its operating temperature. Solar panels normally perform at temperatures above 300 K. Solar cells' operating temperature, on the other hand, might vary throughout production, characterisation, and environmental use. Heights, latitude, time of day in a given location, and season all have an impact on the ambient temperature. As a result, the effect of operating temperature on PSC performance is explored over a temperature range of 250 K to 500 K. Fig.16 shows the measured J-V parameters together with temperature variations. The graph shows how power efficiency slowly increases with growing temperature up to 440 K. As the temperature rises, the V$_{OC}$ decreases because more interfacial defects are formed. The total performance is

optimal at 420 K, with 29.84% of PCE, 1.2596 V of V_{oc}, 87.21% of FF, and 27.16 mA.cm^{-2} of J_{sc}.
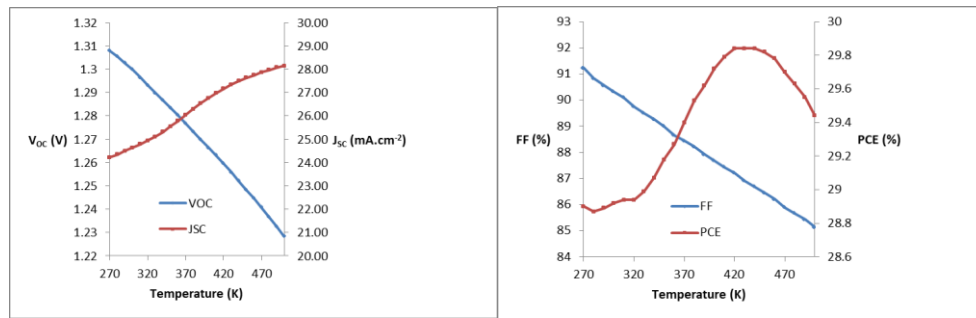


Fig. 16:Influence of temperature on (a) V_{oc}&J_{sc}, (b) PCE & FF.

Influence of series resistance:A series resistance is an internal resistance in a solar cell that inhibits the flow of electricity. The series resistance of a device influences both its FF and short-circuit current density [33]. The passage of current causes bulk resistance, whereas front and back contacts, interfaces, and other points of contact provide series resistance. Variations in series resistance have a major impact on PSC efficiency, suggesting that the lowest attainable series resistance yields the best device performance. Fig. 17 indicates that when the series resistance increasing from 0 to 15 ohm.cm2 reduces the value of PCE from 28.92% to 20.37 percent. FF fell from 90.32 percent to 63.62%. A high series resistance promotes recombination by increasing the voltage drop through the solar cell, making it tougher for charge carriers to reach the electrodes. According to the equation below, the higher the series resistance, the greater the energy loss in a solar cell [34].
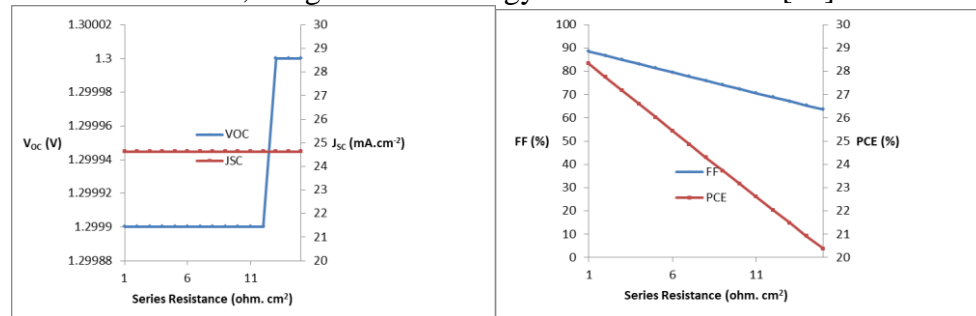

Fig. 17:Influence of series resistance on (a) V_{oc}&J_{sc}, (b) PCE & FF.

Influence of shunt resistance: Every electronic device includes some resistance. Several charge recombination processes produce shunt resistance. To get better performance, much larger shunt resistance is required [35]. A larger shunt resistance indicates that less current is wasted along the parallel channel, subsequent in a more efficient solar cell. The impact of the shunt resistance modelling procedure is investigated. The simulation shows that shunt resistance has relatively little influence on the PSC's performance. In Fig. 18, J_{SC} remains practically constant at 24.63% when we varied the shunt resistance from 10^1 to 10^{15} ohm.cm^2, despite an increase in FFand PCE. The value of PCE increased from 1.52% to 28.92%, while FF increased from 25.00% to 90.32%. This phenomenon happens when the shunt resistance increases, subsequent in a decrease in the amount of current lost owing to shunt recombination, hence increasing both FF and PCE. In most circumstances, a poorly designed PSC device or a manufacturing flaw has a considerable impact on the shunt resistance.
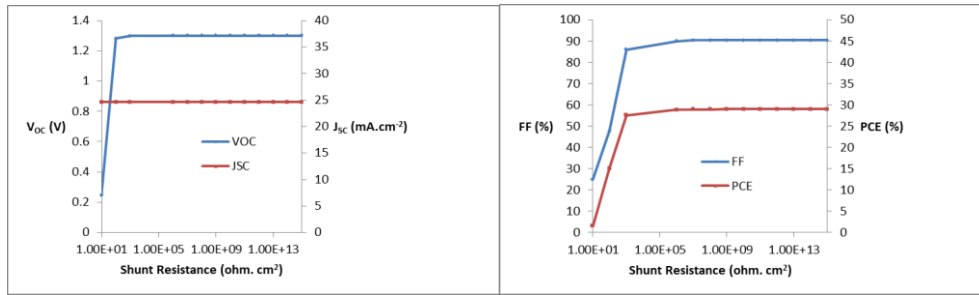
**Fig. 18:Influence of shunt resistance on (a) V_{oc}&J_{sc}, (b) PCE & FF.**

Analysis of quantum efficiency (QE): The quantum efficiency of a PSC is its ability to convert received photons into electrical charge carriers, specifically electrons and holes. QE is determined by the ratio of gathered carriers to photons with certain energy that reach the solar cell [36]. The efficiency can be referring to in terms of wavelength or energy. Fig. 19 depicts how the efficiency of solar cell initially increases with longer wavelengths, reaches a peak, and subsequently decreases. This behaviour happens because the material's quantum characteristics determine how it responds to different wavelengths. As a result, if the wavelength is too short or too long, the efficiency decreases. Solar rays with wavelengths ranging from 370 to 650 nm are generally sufficientto release electrons from their weak bonds and create an electric current. This behaviour is linked to the material's bandgap. Photos with energies over the bandgap are absorbed; however they result in further energy loss as heat, whereas photons below the bandgap are not absorbed. However, due to quantum effects in the material, the exact range may differ. In this simulation, the maximum efficiency is achieved at a wavelength of 380 nm, as illustrated in Fig. 19.
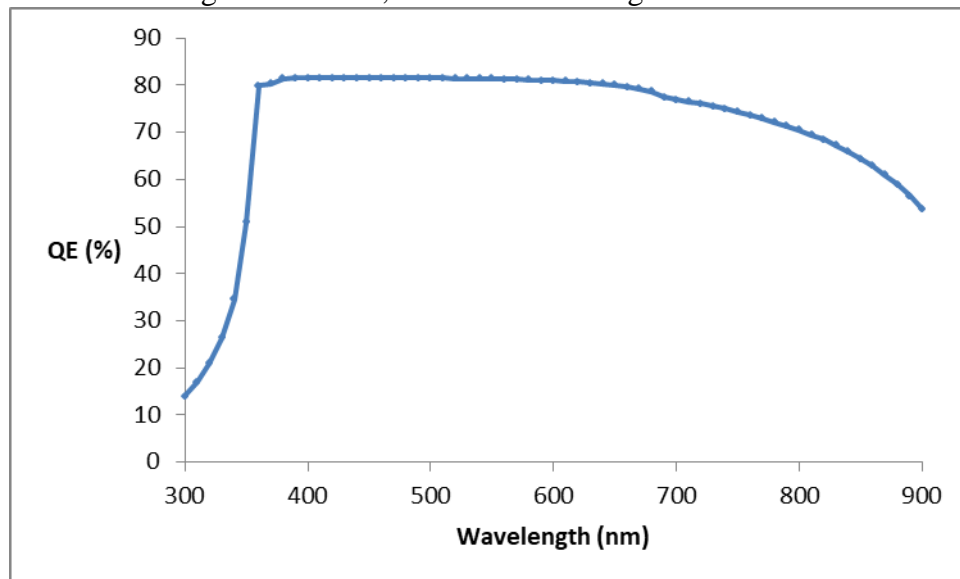
Fig.19: The response of QE concerning incident photon wavelength for the suggested solar cell.

Influence of the work function of back contact material: The back contact material must be tuned to improve the output of PSCs. Its major function is to transmit solar energy to an external circuit. The metal contact offers an ohmic contact for connection, and it must be non-corrosive. Minority charge carriers should have modest recombination rates. PSC allows for the use of a diversity of back contacts, including Ag, Au, Pt, and Pd. The frequently used back contact is Ag, however it has a lower metal work function of 4.2 eV, which might pose instability issues. A significant energy-level discrepancy at the absorber layer/metal contact, which causes the creation of a Schottky junction and lowers device efficiency, may cause the device performance to fall below this work function value [37]. Schottky junction

development can degrade the performance of a PSC. This is because the Schottky junction prevents the charge carrier flow. As a result, selecting an appropriate back contact material with a high value of metal work function is critical for achieving greater efficiency. This is because the electrons from the semiconductor will flow into the metal, bringing their Fermi levels closer to those of the metal. The work function's parameters change from 3.5 to 5.2 eV. Figure 20 demonstrates that for work function 5.1 eV, the maximum PCE of 28.92% occurs for gold (Au). According to this analysis, the work function value should be at least 5.1 eV for enhanced efficiency; performance may suffer if it is lower.
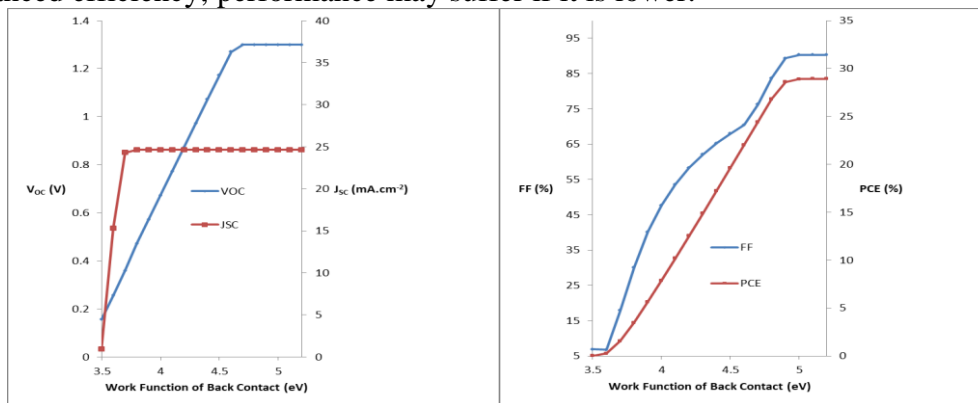
Fig.20: Effect of work-function of back contact on the PCE performance of the proposed structure.

Conclusions: This paper describes a lead-free, ecologically friendly, and stable Cs_2TiBr_6 and $CH_3NH_3SnBr_3$-based all-inorganic PSCs that employs all inorganic charge transport components. The ideal layer thicknesses were determined to build a unique high-performance n-i-p solar cell ($Au/NiO/CH_3NH_3SnBr_3/Cs_2TiBr_6/TiO_2/FTO$). We used SCAPS 1D to theoretically analyse and optimise the suggested solar cell for PV characterisation. After optimizing each layer, a notable efficiency of 28.926%, short circuit current density of 24.63 mA/cm^2, open-circuit voltage of 1.2999 V, and fill factor of 90.32% were obtained. The entire world is shifting towards renewable energy sources. As a result, there are considerable opportunities to design an efficient and cost-effective energy system. The conclusions of presentresearch will not only shed light on the PV process, but will also pave the way for the development of lead-free and efficient solar gadgets. The findings of this work are expected to add to the development of dependable and highly efficient PSCs that do not include lead or other harmful compounds.

Declaration of Competing Interest: The authors state that they have no known competing financial interests or personal relationships that could have influenced the work presented in this study.**Data availability:** Data will be made available on request.

References:

1. NajmulHoque, S.M., Kumar Das, B., Present status of solar home and photovoltaic micro utility systems in Bangladesh and recommendation for further expansion and upgrading for rural electrification. J. Renew. Sustain. Energy 5 (4), 2013, 1–11. https:// doi.org/10.1063/1.4812993.

2. A. Das, S. D. Peu, M. A. M. Akanda, and A. R. M. T. Islam, "Peer-to-Peer Energy Trading Pricing Mechanisms: Towards a Comprehensive Analysis of Energy and Network Service Pricing (NSP) Mechanisms to Get Sustainable Enviro-Economical Energy Sector," Energies, vol. 16, no. 5, 2023, 10.3390/en16052198.

3. Kumar, M., Raj, A., Kumar, A., Anshul, A., Computational analysis of bandgap tuning, admittance and impedance spectroscopy measurements in lead-free MASnI$_3$ perovskite solar cell device. Int. J. Energy Res. 46 (8),2022, 11456–11469. https://doi.org/10.1002/er.7942.

4. I. T. Bello et al., Thickness variation effects on the efficiency of simulated hybrid cu2znsns4-based solar cells using scaps-1d, Biointerface Res. Appl. Chem., vol. 12, no. 6, pp. 7478–7487, 2022, 10.33263/BRIAC126.74787487.

5. Qasim, I., Ahmad, O., ulAbdin, Z., Rashid, A., Farooq Nasir, M., Imran Malik, M., Rashid, M., Hasnain, S.M.,Design and numerical investigations of ecofriendly, non-toxic (Au/CuSCN/CH$_3$NH$_3$SnI$_3$/CdTe/ZnO/ITO) perovskite solar cell and module. Sol. Energy 237, 2022, 52–61.

6. M. Chen, M.G. Ju, A.D. Carl, Y. Zong, R.L. Grimm, J. Gu, X.C. Zeng, Y. Zhou, N.P. Padture, Cesium Titanium(IV) Bromide Thin Films Based Stable Lead-free Perovskite Solar Cells, Joule. 2 (2018) 558–570. https://doi.org/10.1016/j.joule.2018.01.009.

7. F. Igbari, Z.K. Wang, L.S. Liao, Progress of Lead-Free Halide Double Perovskites, Adv. Energy Mater. 9 (2019) 1–32. https://doi.org/10.1002/aenm.201803150.

8. J. Euvrard, X. Wang, T. Li, Y. Yan, D.B. Mitzi, Is Cs$_2$TiBr$_6$ a promising Pb-free perovskite for solar energy applications, J. Mater. Chem. A. 8 (2020) 4049–4054. https://doi.org/10.1039/c9ta13870f.

9. L. Qiao, W.H. Fang, R. Long, Dopant Control of Electron-Hole Recombination in Cesium-Titanium Halide Double Perovskite by Time Domain Ab Initio Simulation: Codoping Supersedes Monodoping, J. Phys. Chem. Lett. 9 (2018) 6907–6914. https://doi.org/10.1021/acs.jpclett.8b03356.

10. W. Li, S. Zhu, Y. Zhao, Y. Qiu, Structure, electronic and optical properties of Cs$_2$Ti(Br$_{1-x}$Y$_x$)$_6$ (Y = Cl, I; x = 0, 0.25, 0.5, 0.75, 1) perovskites: The first principles investigations, J. Solid State Chem. 284 (2020) 121213. https://doi.org/10.1016/j.jssc.2020.121213.

11. K. Chakraborty, M.G. Choudhury, S. Paul, Numerical study of Cs$_2$TiX$_6$ (X = Br−, I−, F− and Cl−) based perovskite solar cell using SCAPS-1D device simulation, Sol. Energy. 194 (2019) 886–892. https://doi.org/10.1016/j.solener.2019.11.005.

12. M. Ju, M. Chen, Y. Zhou, H.F. Garces, J. Dai, N.P. Padture, X.C. Zeng, Earth-Abundant Nontoxic Titanium(IV)-based Vacancy-Ordered Double Perovskite Halides with Tunable 35 1.0 to 1.8 eV Bandgaps for Photovoltaic Applications, ACS Energy Lett. 3 (2018) 297- 304. https://doi.org/10.1021/acsenergylett.7b01167.

13. Mazumder, S., Senthilkumar, K., Device study and optimisation of CZTS/ZnS based solar cell with CuI hole transport layer for different conduction band offset. Sol. Energy 237 (April), 2022, 414–431. https://doi.org/10.1016/j.solener.2022.03.036.

14. A. Das, S. Banik, B.K. Das, A. Das, P. Address, Numerical modeling of lead-free inorganic Cs$_3$Bi$_2$I$_9$ based perovskite solar cell with different charge transport layers and enhancement of device performance by further Investigating the effects of band gap , thickness , carrier density , and defect de, vol. 4313.

15. I. T. Bello et al., "Thickness variation effects on the efficiency of simulated hybrid Cu$_2$ZnSnS$_4$-based solar cells using scaps-1d," Biointerface Res. Appl. Chem., vol. 12, no. 6, pp. 7478–7487, 2022, 10.33263/BRIAC126.74787487.

16. J. Choi, S. Song, M.T. Ho, H.J. Snaith, T. Park, Well-Defined Nanostructured, SingleCrystalline TiO$_2$ Electron Transport Layer for Efficient Planar Perovskite Solar Cells, ACS Nano. 10 (2016) 6029-6036. https://doi.org/10.1021/acsnano.6b01575.

17. W. Ye, J. Xiang, F. Huang, D. Zhong, Towards large-area perovskite solar cells : the influence of compact and mesoporous TiO_2 electron transport layers, Mater. Res. Express. 5 (2018) 085506. https://doi.org/10.1088/2053-1591/aad311 36.

18. T. Dittrich, Porous TiO_2: Electron Transport and Application to Dye Sensitized Injection Solar Cells, phys. stat. sol. (a). 182 (2000) 447–456. https://doi.org/10.1002/1521396X(200011)182:13.0.CO;2-G

19. H. Lu, W. Tian, B. Gu, Y. Zhu, L. Li, TiO_2 Electron Transport Bilayer for Highly Efficient Planar Perovskite Solar Cell, Small. 13 (2017) 1–9. https://doi.org/10.1002/smll.201701535.

20. A.J. Frank, N. Kopidakis, J. Van De Lagemaat, Electrons in nanostructured TiO_2 solar cells : transport, recombination and photovoltaic properties, Coord. Chem. Rev. 248 (2004) 1165–1179. https://doi.org/10.1016/j.ccr.2004.03.015.

21. L. Huang, Z. Hu, J. Xu, X. Sun, Y. Du, J. Ni, H. Cai, Efficient planar perovskite solar cells without a high temperature processed titanium dioxide electron transport layer, Sol. Energy Mater. Sol. Cells. 149 (2016) 1–8. https://doi.org/10.1016/j.solmat.2015.12.033.

22. ArdeshirBaktash, Omid Amiri, AlirezaSasani,Improve efficiency of perovskite solar cells by using Magnesium doped ZnO and TiO_2 compact layers,Superlattices and Microstructures,Volume 93,2016,Pages 128-137, https://doi.org/10.1016/j.spmi.2016.01.026.

23. Kour R, Arya S, Verma S, Gupta J, Bandhoria P, Bharti V, Datt R, Gupta V. Potential Substitutes for Replacement of Lead in Perovskite Solar Cells: A Review. Glob Chall. 2019 Jul 22;3(11):1900050. doi: 10.1002/gch2.201900050. PMID: 31692982; PMCID: PMC6827533.

24. Min Chen, Ming-Gang Ju, Alexander D. Carl, Xiao Cheng Zeng, Yuanyuan Zhou, Nitin P. Padture, Cesium Titanium(IV) Bromide Thin Films Based Stable Lead-free Perovskite Solar Cells; Chen et al., Joule 2, 558–570 March 21, 2018. https://doi.org/10.1016/j.joule.2018.01.009

25. Sobayel K, Akhtaruzzaman M, Rahman KS, Ferdaous MT, Al-Mutairi ZA, Alharbi HF, Alharthi NH, Karim MR, Hasmady S, Amin N. A comprehensive defect study of tungsten disulfide (WS_2) as electron transport layer in perovskite solar cells by numerical simulation. Results in physics. 2019 Mar 1;12:1097-103.

26. Chen, Q., Ni, Y., Dou, X., Yoshinori, Y., The Effect of Energy Level of Transport Layer on the Performance of Ambient Air Prepared Perovskite Solar Cell: A SCAPS1D Simulation Study. Crystals 12 (1), 2022. https://doi.org/10.3390/cryst12010068.

27. A. Islam, N. Bin Alamgir, S. I. Chowdhury, and S. M. B. Billah, "Lead-free organic inorganic halide perovskite solar cell with over 30 % efficiency," vol. 18, no. 3, pp. 395–409, 2022.

28. Mohandes, A., Moradi, M., Nadgaran, H., Numerical simulation of inorganic $Cs_2AgBiBr_6$ as a lead-free perovskite using device simulation SCAPS-1D. Opt. Quant. Electron. 53 (6), 1–22, 2021. https://doi.org/10.1007/s11082-021-02959-z.

29. Hosen, A., Al Ahmed, S.R., Performance analysis of SnS solar cell with a hole transport layer based on experimentally extracted device parameters. J. Alloy. Compd. 909, 2022, 164823.https://doi.org/10.1016/j.jallcom.2022.164823.

30. Alam, I., Ashraf, M.A., Effect of different device parameters on tin-based perovskite solar cell coupled with In_2S_3 electron transport layer and CuSCN and Spiro-OMeTAD alternative hole transport layers for high-efficiency performance. Energy Sources Part A Recover. Util. Environ. Eff. 00 (00), 2020, 1–17. https://doi.org/ 10.1080/15567036.2020.1820628.

31. Mahapatra, B., Krishna, R.V., Laxmi, Patel, P.K., Design and optimization of $CuSCN/CH_3NH_3PbI_3/TiO_2$ perovskite solar cell for efficient performance. Opt. Commun. 504 (August), 2021. https://doi.org/10.1016/j.optcom.2021.127496.

32. Salah, M.M., Abouelatta, M., Shaker, A., Hassan, K.M., Saeed, A., A comprehensive simulation study of hybrid halide perovskite solar cell with copper oxide as HTM. Semicond. Sci. Technol. 34 (11), 2019, 115009.

33. Belarbi, M., Zeggai, O., Louhibi-Fasla, S., Numerical study of Methylammonium Lead Iodide Perovskite solar cells using SCAPS-1D simulation program. Mater. Today: Proc. 51, 2115–2119, 2022. https://doi.org/10.1016/j.matpr.2021.12.425.

34. Jayan,   D.,   High-Efficiency   Non-Toxic   2-Terminal   and   4-Terminal PerovskiteTransition Metal Dichalcogenide Tandem Solar Cells. Adv. Theory Simulations 5 (5), 1–12, 2022. https://doi.org/10.1002/adts.202100611.

35. D. Saikia, J. Bera, A. Betal, and S. Sahu, "Performance evaluation of an all inorganic $CsGeI_3$ based perovskite solar cell by numerical simulation," Opt. Mater. (Amst), vol. 123, no. November 2021, p. 111839, 2022, 10.1016/j.optmat.2021.111839.

36. Chakraborty, K., Choudhury, M.G., Paul, S., Numerical study of Cs_2TiX_6 (X = Br−, I−, F− and Cl−) based perovskite solar cell using SCAPS-1D device simulation. Sol. Energy   194   (November),   886–892,   2019. https://doi.org/10.1016/j.solener.2019.11.005.

37. A. V. Approach, N. Solar, K. K. Maurya, and V. N. Singh, "Comparison of Various ThinFilm-Based Absorber Materials," pp. 2–13, 2022.